Nanocrystalline Chalcopyrite Materials ($CuInS_2$ and $CuInSe_2$) via Low-Temperature Pyrolysis of Molecular Single-Source Precursors

Stephanie L. Castro,*,† Sheila G. Bailey,‡ Ryne P. Raffaelle,§ Kulbinder K. Banger,† and Aloysius F. Hepp‡

Ohio Aerospace Institute, Cleveland, Ohio 44142, Photovoltaics and Space Environments Branch, NASA Glenn Research Center, Cleveland, Ohio 44135, and Department of Physics, Rochester Institute of Technology, Rochester, New York 14623

Received March 14, 2003. Revised Manuscript Received May 19, 2003

Nanometer-sized particles of the chalcopyrite compounds $CuInS_2$ and $CuInSe_2$ were synthesized by thermal decomposition of molecular single-source precursors $(PPh_3)_2CuIn(SEt)_4$ and $(PPh_3)_2CuIn(SePh)_4$, respectively, in the noncoordinating solvent dioctyl phthalate at temperatures between 200 and 300 °C. The nanoparticles range in size from 3 to 30 nm and are aggregated to form roughly spherical clusters of about 500 nm in diameter. X-ray diffraction of the nanoparticle powders shows greatly broadened lines, indicative of very small particle sizes, which is confirmed by TEM. Peaks present in the XRD can be indexed to reference patterns for the respective chalcopyrite compounds. Optical spectroscopy and elemental analysis by energy dispersive spectroscopy support the identification of the nanoparticles as chalcopyrites.

Introduction

The space photovoltaic community is well aware of the cost benefits to both mission and spacecraft development associated with the continued increase in solar cell efficiency. Over the past decade much of the cell efficiency improvements have resulted from the move toward multijunction devices.

Chalcopyrite-based photovoltaic devices $(Cu(In:Ga)(S:Se)_2)$ have been a focus of the space photovoltaic community for over 2 decades.[1−3] Thin-film photovoltaic devices made with the chalcopyrite semiconductors are expected to be highly efficient. Thin-film $CuInS_2$ cells with efficiencies of 12.5% have been successfully produced,[4] and efficiencies up to 18.8% have been recorded for $Cu(In, Ga)Se_2$-based cells.[5] The band gap of $CuInS_2$ ($E_g = 1.5$ eV) is well-matched to the AM0 solar spectrum for photovoltaic performance. Although $CuInSe_2$ ($E_g = 1.1$ eV) is not as well-matched, other attributes such as a high absorption coefficient and low-cost methods for deposition of thin films make $CuInSe_2$ a promising material for photovoltaic devices.

As researchers continue to push the envelope, they are looking to new approaches, such as the use of nanotechnology, to improve device performance. Future photovoltaic devices may employ materials such as semiconductor quantum dots. Quantum dots are nanometer-sized particles whose small size allows for three-dimensional size confinement of the bulk energy bands into discrete, molecular-like energy states. In this size regime, the band gap of a material can be "tuned" to a desired energy by adjusting the particle size, offering the possibility of growing quantum dots to match a specific region of the solar spectrum. The inclusion of nanocrystalline materials in photovoltaic devices[6] has been proposed to improve the efficiency of photon conversion (intermediate band solar cell)[7−10] and provide sites for exciton dissociation and pathways for electron transport.[11−16] Luque and Martí[7] proposed an

* Corresponding author: Stephanie Castro, c/o NASA Glenn Research Center, Mail Stop 302-1, 21000 Brookpark Rd., Cleveland, OH 44135. E-mail: stephanie.castro@grc.nasa.gov.

† Ohio Aerospace Institute.

‡ NASA Glenn Research Center.

§ Rochester Institute of Technology.

(1) Bailey, S. G.; Flood, D. J. *Prog. Photovoltaics: Res. Appl.* **1998**, *6*, 1−14.

(2) Schock, H. W.; Noufi, R. *Prog. Photovoltaics: Res. Appl.* **2000**, *8*, 151−160.

(3) Schock, H. W.; Bogus, K. Development of CIS solar cells for space applications. In *Proceedings of the Second World Conference on Photovoltaic Energy*; Schmid, J., Ossenbrink, H. A., Helm, P., Ehmann, H, Dunlop, E. D., Eds.; EC Joint Research Center: Luxembourg, 1998; pp 3586−3589.

(4) Klaer, J.; Bruns, J.; Henninger, R.; Töpper, K.; Klenk, R.; Ellmer, K.; Bräunig, D. In *Proceedings of the Second World Conference on Photovoltaic Solar Energy Conversion*; Schmid, J., Ossenbrink, H. A., Helm, P., Ehmann, H., Dunlop, E. D., Eds.; EC Joint Research Center: Luxembourg, July 1998; pp 537−540. A tolerant two-step process for efficient $CuInS_2$ solar cells.

(5) Contreras, M. A.; Egaas, B.; Ramanathan, K.; Hiltner, J.; Swartzlander, A.; Hasoon, F.; Noufi, R. *Prog. Photovoltaics: Res. Appl.* **1999**, *7*, 311−316.

(6) A collection of reviews on this topic is available in a special issue of *Physica E* (**2002**, *14*, issue 1−2) entitled "Nanostructures in Photovoltaics".

(7) (a) Luque, A.; Martí, A. *Phys. Rev. Lett.* **1997**, *78*, 5014−5017. (b) Martí, A.; Cuadra, L.; Luque, A. Quantum Dot Intermediate Band Solar Cell. In *Twenty-eighth IEEE Proceedings of the Photovoltaics Specialists Conference*, Anchorage, Alaska, September 2000; IEEE: New York, 2000; pp 940−943.

(8) Aroutiounian, V.; Petrosyan, S.; Khachatryan, A.; Touryan, K. *J. Appl. Phys.* **2001**, *89*, 2268−2271.

(9) Raffaelle, R. P.; Castro, S. L.; Hepp, A. F.; Bailey, S. G. *Prog. Photovoltaics: Res. Appl.* **2002**, *10*, 433−439.

(10) Brown, A. S.; Green, M. A.; Corkish, R. P. *Physica E* **2002**, *14*, 121−125.

10.1021/cm034161o CCC: $25.00
Published on Web 06/27/2003

"intermediate band solar cell" (IBSC) with a theoretical efficiency of over 63%, well in excess of the most efficient cells available today. New calculations by Brown et al.[10] increase the number of bands in the Luque model from three to four and find a concomitant increase in efficiency to 71.7%. Composites of quantum dots and conductive organic polymers[11,12,16] have been employed to overcome some of the limitations of charge transport efficiency due to low electron mobility in conjugated organic polymers. Quantum dots are also more resistant to degradation from electron, proton, and alpha particle radiation than the corresponding bulk material, preferred characteristics for use in space solar cells.[17−19]

The possibilities of increased efficiency and resistance to radiation-induced defects led us to investigate quantum dots as part of our ongoing research on chalcopyrite materials for space photovoltaic applications. In contrast to the overall quantity of quantum dot research[20] in the literature, relatively few reports[21−29] have been published about the synthesis of nanosized I−III−VI_2 ternary materials $CuInS_2$ and $CuInSe_2$.

Colloidal synthesis of nanoparticles offers greater control over morphology and size than do MOCVD (metal−organic chemical vapor deposition) methods, particularly for very small particles. In the past decade, synthetic control over colloidal nanoparticles has greatly improved, especially for the II−VI and III−V semiconductors.[30] Recent work by O'Brien and co-workers[31] and Strouse and co-workers[32] with single-source precursors has shown them to be viable starting materials for the synthesis of high-quality colloidal quantum dots. Single-source precursors are discrete molecules that include all the elements required in the final material. These precursors can be designed with many properties in mind, including stoichiometry, solubility, and volatility. Our group has studied the synthesis of single-source precursors to $CuInS_2$ and $CuInSe_2$, and the subsequent conversion of these precursors to thin films of the bulk semiconducting materials.[33−36] The molecular precursor $(PPh_3)_2CuIn(SEt)_4$ (Figure 1) was first described by Hirpo et al. in 1993.[37] This charge-neutral molecule comprises a copper(I) ion bound by two triphenylphosphine ligands, an indium(III) ion with two terminal ethanethiolate ligands, and two ethanethiolate ligands coordinated in a *m*2-bridging manner between the metal centers.

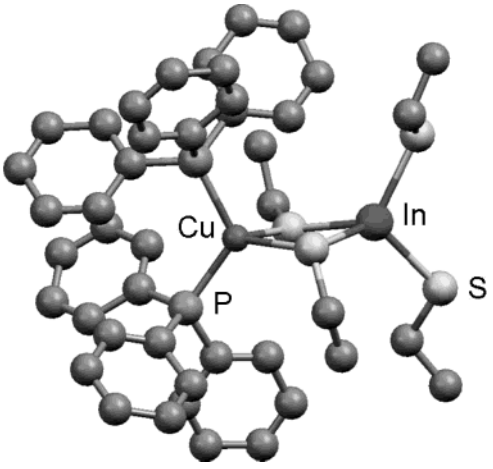

Figure 1. Molecular structure of $(PPh_3)_2CuIn(SEt)_4$.

In this study, the precursor $(PPh_3)_2CuIn(SEt)_4$ (**1**) was used in the synthesis of $CuInS_2$ nanoparticles. The analogous compound $(PPh_3)_2CuIn(SePh)_4$ (**1′**) was used in the synthesis of $CuInSe_2$ nanoparticles. To the best of our knowledge, this paper presents the first reported use of a ternary single-source precursor to synthesize chalcopyrite nanoparticles.

(11) (a) Huynh, W. U.; Peng, X.; Alivisatos, A. P. *Adv. Mater.* **1999**, *11*, 923−927. (b) Huynh, W. U.; Dittmer, J. J.; Alivisatos, A. P. *Science* **2002**, *295*, 2425−2427.

(12) (a) Arici, E.; Hoppe, H.; Reuning, A.; Sariciftci, N. S.; Meissner, D. CIS Plastic Solar Cells. In *Seventeenth European Photovoltaic Solar Energy Conference Proceedings*, Munich, Germany, 2001; James and James Ltd.: London, 2001. CIS plastic solar cells. (b) Arici, E.; Sariciftci, N. S.; Meissner, D. *Mol. Cryst. Liq. Cryst.* **2002**, *385*, 249−256.

(13) Grätzel, M. *Prog. Photovoltaics: Res. Appl.* **2000**, *8*, 171−185.

(14) Wang, Y.; Herron, N. *J. Lumin.* **1996**, *70*, 48−59.

(15) (a) Nozik, A. J. *Annu. Rev. Phys. Chem.* **2001**, *52*, 193−231. (b) Nozik, A. J. *Physica E* **2002**, *14*, 115−120.

(16) (a) Godovsky, D. Y.; Varfolomeev, A. E.; Zaretsky, D. F.; Chandrakanthi, R. L. N.; Kündig, A.; Weder, C.; Caseri, W. *J. Mater. Chem.* **2001**, *11*, 2465−2469. (b) Chandrakanthi, R. L. N.; Careem, M. A. *Thin Solid Films* **2002**, *417*, 51−56.

(17) Marcinkevičius, S.; Leon, R.; Čechavičius, B.; Siegert, J.; Lobo, C.; Magness, B.; Taylor, W. *Physica B* **2002**, *314*, 203−206.

(18) Walters R. J.; Summers, G. P.; Messenger, S. R.; Freundlich, A.; Monier, C.; Newman, F. *Prog. Photovoltaics: Res. Appl.* **2000**, *8*, 349−354.

(19) Sobolev, N. A.; Cavaco, A.; Carmo, M. C.; Grundmann, M.; Heinrichsdorff, F.; Bimberg, D. *Phys. Status Solidi B* **2001**, *224*, 93−96.

(20) A search of the term "quantum dot*" in the Science Citation Index in March 2003 yielded 10,800 hits.

(21) Malik, M. A.; O'Brien, P.; Revaprasadu, N. *Adv. Mater.* **1999**, *11*, 1441−1444.

(22) Czekelius, C.; Hilgendorff, M.; Spanhel, L.; Bedja, I.; Lerch, M.; Müller, G.; Bloeck, U.; Su, D.-S.; Giersig, M. *Adv. Mater.* **1999**, *11*, 643−646.

(23) Gurin, V. S. *Colloids Surf. A* **1998**, *142*, 35−40.

(24) (a) Lu, Q.; Hu, J.; Tang, K.; Qian, Y.; Zhou, G.; Liu, X. *Inorg. Chem.* **2000**, *39*, 1606−1607. (b) Cui, Y.; Ren, J.; Chen, G.; Qian, Y.; Xie, Y. *Chem. Lett.* **2001**, 236−237. (c) Jiang, Y.; Wu, Y.; Yuan, S.; Xie, B.; Zhang, S.; Qian, Y. *J. Mater. Res.* **2001**, *16*, 2805−2809.

(25) Gurinovich, L. I.; Gurin, V. S.; Ivanov, V. A.; Bodnar, I. V.; Molochko, A. P.; Solovej, N. P. *Phys. Status Solidi B* **1998**, *208*, 533−540.

(26) Malyarevich, A. M.; Yumashev, K. V.; Posnov, N. N.; Mikhailov, V. P.; Gurin, V. S.; Prokopenko, V. B.; Alexeenko, A. A.; Melnichenko, I. M. *J. Appl. Phys.* **2000**, *87*, 212−216.

(27) Jiang, Y.; Wu, Y.; Mo, X.; Yu, W.; Xie, Y.; Qian, Y. *Inorg. Chem.* **2000**, *39*, 2964−2965.

(28) (a) Xiao, J.; Xie, Y.; Tang, R.; Qian, Y. *J. Mater. Chem.* **2001**, *11*, 1417−1420. (b) Xiao, J.; Xie, Y.; Tang, R.; Qian, Y. *J. Solid State Chem.* **2001**, *161*, 179−183. (c) Li, B.; Xie, Y.; Huang, J.; Qian, Y. *Adv. Mater.* **1999**, *11*, 1456−1459.

(29) Mandale, A. B.; Sathaye, S. D.; Patil, K. R. *Mater. Lett.* **2002**, *55*, 30−33.

(30) For reviews of this topic see: Murray, C. B.; Kagan, C. R.; Bawendi, M. G. *Annu. Rev. Mater. Sci.* **2000**, *30*, 545−610, and Trindade, T.; O'Brien, P.; Pickett, N. L. *Chem. Mater.* **2001**, *13*, 3843−3858.

(31) (a) Trindade, T.; O'Brien, P. *Adv. Mater.* **1996**, *8*, 161. (b) Trindade, T.; O'Brien, P.; Zhang, X. *Chem. Mater.* **1997**, *9*, 523−530. (c) Malik, M. A.; Revaprasadu, N.; O'Brien, P. *Chem. Mater.* **2001**, *13*, 913−920.

(32) Cumberland, S. L.; Hanif, K. M.; Javier, A.; Khitrov, G. A.; Strouse, G. F.; Woessner, S. M.; Yun, C. S. *Chem. Mater.* **2002**, *14*, 1576−1584.

(33) (a) Banger, K. K.; Cowen, J.; Hepp, A. F. *Chem. Mater.* **2001**, *13*, 3827−3829. (b) Banger, K. K.; Harris, J. D.; Cowen, J. E.; Hepp, A. F. *Thin Solid Films* **2002**, *403−404*, 390−395. (c) Banger, K. K.; Hollingsworth, J. A.; Harris, J. D.; Cowen, J.; Buhro, W. E.; Hepp, A. F. *Appl. Organomet. Chem.* **2002**, *16*, 617−627.

(34) Henderson, D. O.; Mu, R.; Ueda, A.; Wu, M. H.; Gordon, E. M.; Tung, Y. S.; Huang, M.; Keay, J.; Feldman, L. C.; Hollingsworth, J. A.; Buhro, W. E.; Harris, J. D.; Hepp, A. F.; Raffaelle, R. P. *Mater. Des.* **2001**, *22*, 585−589.

(35) Raffaelle, R. P.; Potdevin, T.; Hepp, A. F.; Bailey, S. G. *Mater. Sci., Semicon. Process.* **1999**, *2*, 289−296.

(36) Hollingsworth, J. A.; Hepp, A. F.; Buhro, W. E. *Chem. Vap. Deposition* **1999**, *5*, 105−108.

Experimental Section

Materials. $(PPh_3)_2CuIn(SEt)_4$ (**1**) and $(PPh_3)_2CuIn(SePh)_4$ (**1′**) were prepared by literature methods.[33a] The starting materials are slightly air-sensitive and are stored in an argon-filled inert atmosphere drybox (Vac Atmospheres) to prevent decomposition. As synthesized, the precursors are white to light yellow in color and give satisfactory elemental analyses. Standard air-sensitive (Schlenk) techniques were employed during synthesis. Dioctyl phthalate (99+%) was purchased from ACROS and used without further purification. Methanol (Optima grade) and toluene (HPLC grade) were purchased from Fisher Scientific and used without further purification.

Measurement. Optical spectra were recorded on a Perkin-Elmer Lambda 19 spectrophotometer; samples were embedded on 3M brand Scotch Tape for analysis. Scanning electron microscopy (SEM) was performed on an Hitachi S3000N microscope operating at 25 kV; samples were prepared by dispersing a few milligrams of powder in methanol or toluene prior to dropping on an aluminum support (SPI) and allowing the solvent to evaporate. Elemental analyses were collected with an EDAX energy-dispersive X-ray spectrometer (EDS) operating at 25 kV. The results were quantitated by ZAF standardless correction. High-resolution transmission electron microscopy (HRTEM) was performed on a Philips CM200 operating at 200 kV in bright field mode. The digital image was collected on a Gatan Imaging Filter (GIF 1024 × 1024 pixels). The magnification was calibrated using the Mag*i*cal TEM standard (http://www.emsdiasum.com/ems/calibration/magical.html). The TEM grids were Ted Pella 01881 lacey carbon; samples were prepared by dipping the grid into a milliliter of methanol containing suspended nanocrystalline powder and allowing the methanol to evaporate. Powder X-ray diffraction patterns were obtained on a Philips X'Pert diffractometer using Cu Kα radiation, excited at 45 kV and 40 mA. The X-rays were collimated at the source with a 10-mm mask and divergence slit set at 1° and at the detector with a 2-mm receiving slit and antiscatter slit set to 1°.

Preparation of $CuInS_2$ Nanoparticles. Dioctyl phthalate (10 mL) was heated to 125 °C under vacuum for 1 h to dry and degas the solvent; the flask was back-filled with argon and cooled to room temperature prior to adding the precursor. $(PPh_3)_2CuIn(SEt)_4$ (1.945 g, 2.0 mmol) was added to the reaction flask and heating was resumed. At approximately 150 °C the precursor dissolved to form a transparent yellow solution; no further change was observed with time at this temperature. At this point the solution could be returned to room temperature without reprecipitation of the precursor. The yellow color is likely due to a trace amount of decomposition or impurity; the absorption spectrum of the yellow dioctyl phthalate solution is indistinguishable from that of a toluene solution of the precursor. In addition, the precursor can be recovered in near-quantitative yield by addition of hexanes to the yellow dioctyl phthalate solution. At 150 °C, the precursor remains, for the most part, intact. Upon increase of the temperature to 200 °C an as-yet unidentified (see Discussion) red powder (product **2**) began to precipitate within a few minutes; a reaction time of 2 h was employed to complete the precipitation and maximize the yield. After cooling to room temperature under argon, toluene (40 mL) was added to the reaction mixture to lower the viscosity of the reaction mixture and the red powder was isolated by centrifugation. The powder was consecutively washed with toluene and methanol to remove reaction byproducts and unreacted starting material and was dried under vacuum at 60 °C. The washing and centrifugation steps were carried out in ambient atmosphere. The product appeared only slightly air-sensitive at room temperature; a green tinge was observed on the surface of the powder after several weeks in ambient laboratory atmosphere. Then 0.427 g of **2** was collected and stored in a glovebox.

A portion of **2** (100 mg) was placed in a flask containing fresh dioctyl phthalate (10 mL), heated to higher temperatures, 250 or 300 °C, and held for 1 h. When the temperature was 250 °C, a brown/black powder ($CuInS_2$, **3**) was obtained; at 300 °C the resulting powder was black ($CuInS_2$, **4**). Each powder was washed and dried in the same manner before analysis. **3** and **4** are both identified as nanocrystalline $CuInS_2$ by XRD.

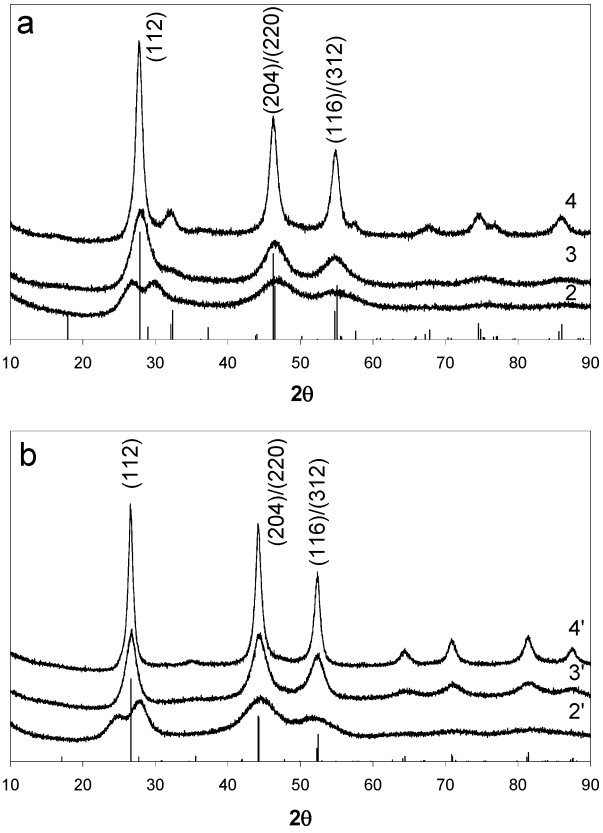

Figure 2. Powder XRD patterns for (a) **2**, **3**, and **4**, the reaction products of $(PPh_3)_2CuIn(SEt)_4$ at 200, 250, and 300 °C, respectively. Reference pattern 85-1575 ($CuInS_2$) is shown along the *x*-axis. (b) **2′**, **3′**, and **4′**, the reaction products of $(PPh_3)_2CuIn(SePh)_4$ at 200, 275, and 300 °C, respectively. Reference pattern 87-2265 ($CuInSe_2$) is shown along the *x*-axis.

Preparation of $CuInSe_2$ Nanoparticles. The same procedure as above was followed for the $CuInSe_2$ precursor, but the precursor dissolved in the dioctyl phthalate at 138 °C. $(PPh_3)_2CuIn(SePh)_4$ (1.951 g, 1.47 mmol) was dissolved in 10 mL of dioctyl phthalate. A red powder (0.523 g, product **2′**) was collected after 2 h of heating at 200 °C. At 250 °C, the XRD pattern (Figure 2b) of the resulting selenium-containing powder still exhibited substantial splitting of the 112 line (vide infra); temperatures of 275 and 300 °C were employed for the second and third steps, giving products **3′** and **4′**, respectively. **3′** and **4′** are identified as CuInSe2 by XRD, **2′** is as yet unidentified (see Discussion).

Results

X-ray Diffraction. XRD (Figure 2) clearly shows pure $CuInS_2$ is the product of the reaction at 250 and 300 °C and $CuInSe_2$ at 275 and 300 °C. Each peak in the diffraction pattern can be indexed to the appropriate reference pattern (JCDPS #85-1575, $CuInS_2$, and #87-2265, $CuInSe_2$). In every pattern, significant broadening of the diffraction lines is apparent; average particle sizes of 2.85(5) and 7.4(4) nm were calculated by the Scherrer formula based on two peaks for **3** and **4** and 4.4(4) and 9.8(6) nm for **3′** and **4′**, respectively. The Scherrer formula is known to be uncertain for X-ray patterns with overlapping peaks, and the size distributions

(37) Hirpo, W.; Dhingra, S.; Sutorik, A. C.; Kanatzidis, M. G. *J. Am. Chem. Soc.* **1993**, *115*, 1597−1599.

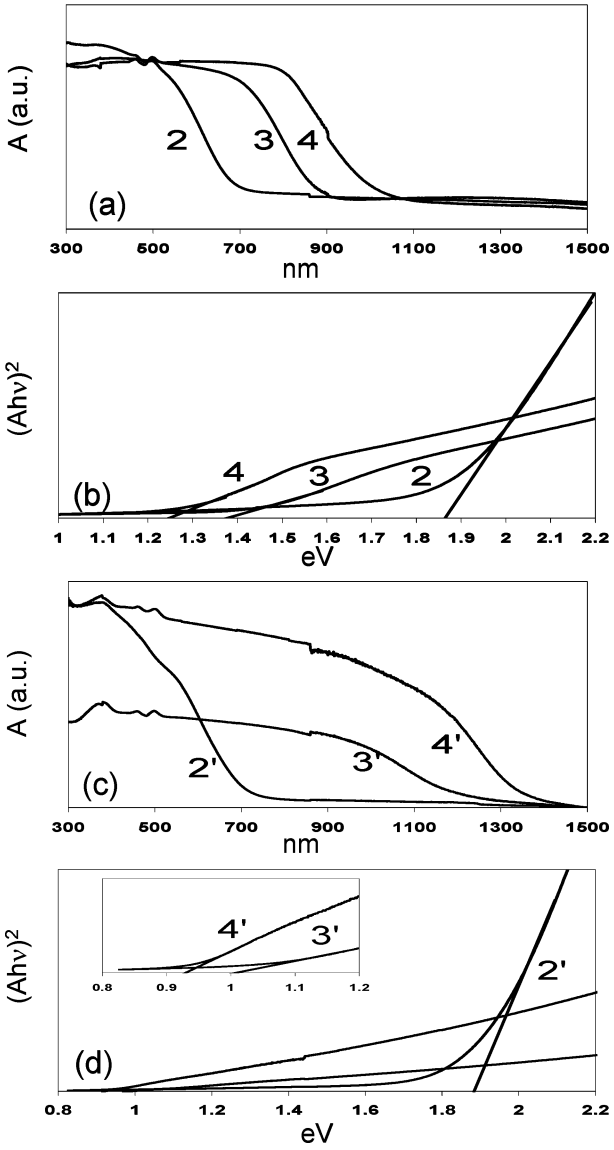

Figure 3. (a) Absorption spectra of products **2**, **3**, and **4**; (c) absorption spectra of products **2′**, **3′**, and **4′**; (b) plots of $(Ah\nu)^2$ vs energy for products **2**, **3**, and **4**; (d) plots of $(Ah\nu)^2$ vs energy for products **2′**, **3′**, and **4′**. Straight lines represent the least-squares best fit to the linear region of the plot; the inset in plot (d) shows the expanded region around the *x*-axis for products **3′** and **4′**.

observed by electron microscopy (vide infra) are broad. However, the combination of the two techniques strongly supports the conclusion that the average particle size increases with higher reaction temperatures.

The XRD patterns of **2** and **2′** contain two peaks roughly centered about the expected (112) position; the remaining two index peaks (204/220) and (116/312) are in their expected positions. An analysis of this observation is presented in the Discussion section.

Optical Spectroscopy. Absorption spectra of **2**, **3**, and **4** (Figure 3a,b) and **2′**, **3′**, and **4′** (Figure 3c,d) immobilized on matte adhesive tape exhibited shifts of the absorption onsets relative to the $CuInS_2$ bulk band gap of 1.5 eV or $CuInSe_2$ at 1.1 eV. The absorption onset of each product was determined by a least-squares fit of the linear region of a $(Ah\nu)^2$ vs $h\nu$ plot (A = absorbance, h = Planck's constant, and ν = frequency).[38−40] The values for all products are listed in Table 1.

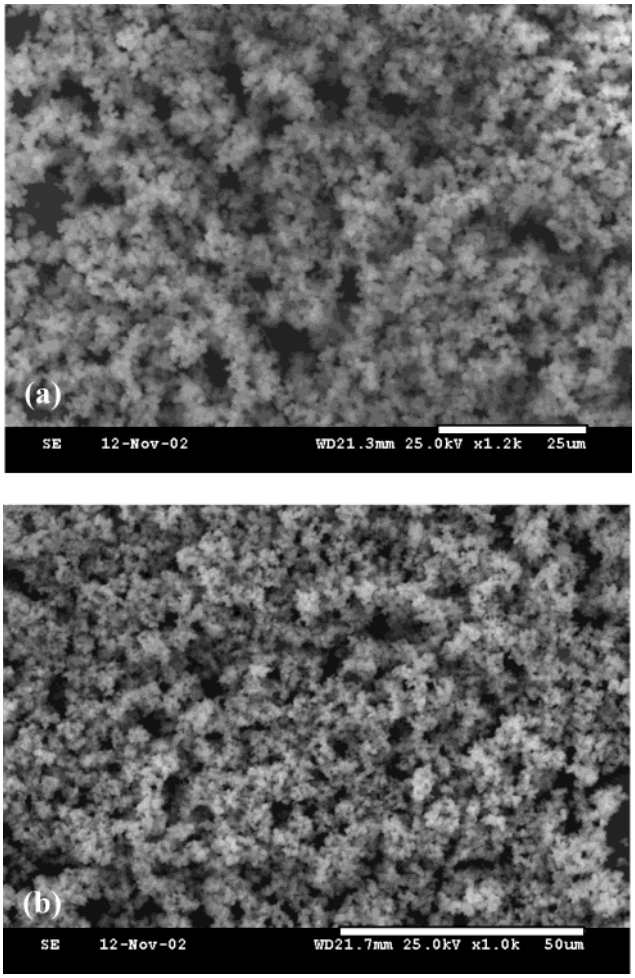

Figure 4. SEM images of (a) **2** and (b) **4**. Scale bars are 25 and 50 μm, respectively.

Table 1. Absorption Onset Energies for Powdered Samples Immobilized on Adhesive Tape

sample	absorption onset energy (eV)	sample	absorption onset energy (eV)
2	1.86(2)	**2′**	1.88(3)
3	1.38(3)	**3′**	1.01(1)
4	1.25(5)	**4′**	0.93(1)

Electron Microscopy. The powders were examined by scanning and transmission electron microscopies. SEM of all powders shows large spherical particles of ∼500-nm diameter. Typical images are shown in Figure 4. At higher resolution, the large particles were observed to be aggregates of nanoparticles, as seen in Figure 5. From the HRTEM images, the size distribution of the samples appears broad.

Discussion

On the basis of our early success with the single-source precursors for chalcopyrite thin films,[33−36] we focused our efforts on the transformation of these precursors to colloidal chalcopyrite quantum dots. Initial attempts to use the "hot surfactant method" of colloidal

(38) Onnagawa, H.; Miyashita, K. *Jpn. J. Appl. Phys.* **1984**, *23*, 965−969.
(39) Shay, J. L.; Wernick, J. H. *Ternary Chalcopyrite Semiconductors*; Pergamon: Oxford, 1975; p 118.
(40) Rajaram, P.; Thangaraj, R.; Sharma, A. K.; Raza, A.; Agnihotri, O. P. *Thin Solid Films* **1983**, *100*, 111−116.

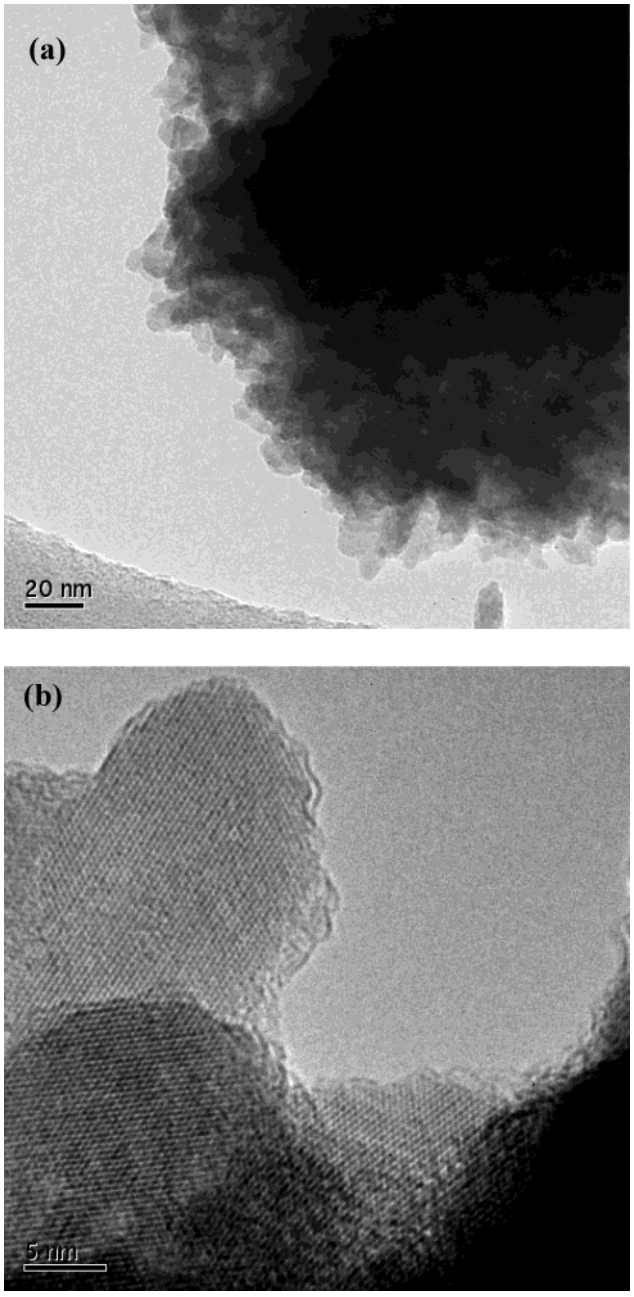

Figure 5. Medium (a) and high-resolution (b) TEM images of **4**. Scale bars are 20 and 5 nm, respectively.

nanoparticle synthesis failed. This method, pioneered by Murray et al. in 1993,[41] involves injection of a precursor(s) dissolved in a solvent into a surfactant heated to ~300 °C. A persistent theme in the choice of surfactant is that it has metal-coordinating properties, although recent results from the Peng group show a possible avenue away from this restriction.[42] Injection of the $CuInS_2$ precursor into common coordinating solvents such as trioctylphosphine, oleic acid, stearic acid, or hexadecylamine, or some combinations of these, led to separation of the precursor components into binary materials such as copper sulfide. It is also possible that during dissolution in trioctylphosphine, the precursor loses its molecular integrity, with the phosphine solvent participating in the copper ligation and breaking apart the precursor. In the spray pyrolysis process for which the precursors were developed, the working solvent is toluene, and the precursors have good solubility without decomposition (at room temperature). For this reason, we then moved to a noncoordinating solvent. Dioctyl phthalate was chosen based on its boiling point (384 °C).

Scheme 1. Reaction Scheme for the Conversion of the Single-Source Precursors to $CuInS_2$ and $CuInSe_2$

SYNTHESIS OF NANOCRYSTALLINE $CuInS_2$ AND $CuInSe_2$ FROM SINGLE-SOURCE PRECURSORS

$(PR_3)_2CuIn(ER')_4$ —Dioctyl phthalate, 200 °C→ **2** (R = C_6H_5; R' = $-CH_2CH_3$; E = S); **2'** (R = C_6H_5; R' = $-C_6H_5$; E = Se)

2 and **2'** are red-brown powders. Each is washed with toluene and methanol to remove unreacted precursor, dried under vacuum, and stored in a glove box for future use.

2 —Dioctyl phthalate, 250 °C→ **3**; **2'** —Dioctyl phthalate, 275 °C→ **3'**

2 —Dioctyl phthalate, 300 °C→ **4**; **2'** —Dioctyl phthalate, 300 °C→ **4'**

The precursors dissolved completely in dioctyl phthalate with moderate heating to form a yellow solution (the precursor in the solid state is white to light yellow), and began to change to orange and red at 200 °C, followed immediately by precipitation. A disadvantage of a noncoordinating solvent is the solvent cannot act as a surfactant, binding to the surface of the growing nanocrystal and preventing aggregation with its neighbors. SEM and TEM showed the precipitate to be made up of large clusters of smaller nanocrystals. Future work includes postprocessing alteration of the surface of the nanoparticles to enable dispersion in organic solvents and subsequent narrowing of the size distributions by size-selective precipitation.[41] A surfactant-passivated nanocrystal surface allows for controlled growth of colloidal nanocrystals.

The stepwise method of synthesis, isolating the red intermediate before raising the temperature, was critical for the purest products. If the precursor was brought directly to 250 or 300 °C, the final black powder was predominantly $CuInS_2$, but impurity peaks were evident in the XRD pattern. The reactions are outlined in Scheme 1.

We were unable to conclusively determine the identity of **2** or **2′**. We hypothesized that the red material could be an intermediate precursor comprising a mixture of Cu_xE_y and In_xE_y (E = S or Se), which could recombine at higher temperatures to form $CuInE_2$. An extensive search of the JCPDS-ICDD XRD database, focusing especially on the binary and ternary mixtures of Cu, In, and S or Se, found no clear matches to known phases which incorporated all the features observed in the experimental patterns while omitting no major peaks from the reference pattern.

Qualitative analysis supports the conclusion that copper sulfide is not a significant component of **2**. It is

(41) Murray, C. B.; Norris, D. J.; Bawendi, M. G. *J. Am. Chem. Soc.* **1993**, *115*, 8706−8715.
(42) Yu, W. W.; Peng, X. *Angew. Chem., Int. Ed.* **2002**, *41*, 2368−2371.

well-established that covellite (CuS, more accurately represented as the mixed-valence compound $Cu^{I}_4Cu^{II}_2(S_2)_2S_2$[43]) is dissolved by aqueous KCN solutions.[44] A sample of **2** was washed with 1% KCN for two 10-min periods with gentle agitation. The sample was washed thoroughly with distilled water and dried under vacuum. The XRD pattern of the product was completely unaffected by the KCN wash. Investigation into the identity of **2** and **2′** is ongoing. It is important to note though that identification of these products is not critical to this report, as both **2** and **2′** are cleanly converted to the desired chalcopyrite materials at higher reaction temperatures (250 and 275 °C, respectively).

Optical spectroscopy was also employed to characterize the nanocrystals. An increase in band gap energy is one of the characteristics of size quantization in semiconductor nanoparticles. However, the absorption onsets for **3**, **4**, **3′**, and **4′** are at lower energy than those of the bulk band gaps. The onset for **3** is ~1.38 eV, and **4** is ~1.2 eV. Sub-bandgap absorption is not uncommon for $CuInE_2$ (E = S, Se); it has been observed in thin films and polycrystalline samples. It can be attributed to surface defects and grain boundaries. In theory, both of these should diminish in importance with increasing sample preparation temperature, as the particles should both increase in size and defects at the surface should anneal out. The apparent opposite is observed here. The onset of absorption for **4** (prepared at 300 °C) shows sub-bandgap absorption at even lower energy than for **3** (prepared at 250 °C). The same trend is observed for the $CuInSe_2$ powders; see Figure 3c,d. These observations are likely due to the relatively low synthesis temperatures compared to the typical bulk annealing temperatures at 600−700 °C.

Elemental analysis by ZAF standardless correction (Table 2) of the powders by EDS (energy-dispersive spectroscopy) shows Cu:In:S(Se) ratios close to those expected for the products.

Table 2. Elemental Ratio in Products Determined by EDS

sample	Cu	In	S (Se)
2	1.0	0.91(6)	2.3(3)
3	1.0	0.89(1)	1.58(4)
4	1.0	0.94(2)	1.8(1)
2′	1.0	1.18(4)	(3.09(6))
3′	1.0	1.11(6)	(2.2(1))
4′	1.0	1.03(6)	(2.27(7))

Conclusion

The CVD precursors $(PPh_3)_2CuIn(SEt)_4$ and $(PPh_3)_2CuIn(SePh)_4$ can be converted to nanocrystalline chalcopyrite materials $CuInS_2$ and $CuInSe_2$, respectively, by pyrolysis in a noncoordinating solvent. The conversion takes place in two steps: first by formation of an as-yet unidentified red intermediate and then by further transformation to the chalcopyrite structure. The identity of the material is confirmed by powder X-ray diffraction; evidence of the nanometer-scale particle diameters is confirmed by TEM. The average size of the nanoparticles as determined by TEM, as well as the lack of a blue shift in the absorption energy of products **3**, **4**, **3′**, and **4′**, indicates that the particles are likely not small enough to exhibit size quantization effects and, although nanoparticles, are not truly "quantum dots". The Bohr exciton radii[45] of $CuInS_2$ and $CuInSe_2$ are 4.1 and 10.6 nm, respectively. The material is largely aggregated; however, we are optimistic that these precursors may yet provide a route to colloidal chalcopyrite quantum dots.

Acknowledgment. This work was supported by NASA Glenn Research Center Strategic Research Fund; NASA Cooperative Agreements NCC3-958, NCC3-710, and NCC3-563; Rochester Institute of Technology and Ohio Aerospace Institute.

CM034161O

(43) Robbins, M.; Bachmann, K. J.; Lambrecht, V. G.; Thiel, F. A.; Thomson, J.; Vadimsky, R. G.; Menezes, S.; Heller, A.; Miller, B. *J. Electrochem. Soc.* **1978**, *125*, 831−832.

(44) Weber, M.; Scheer, R.; Lewerenz, H. J.; Jungblut, H.; Störkel, U. *J. Electrochem. Soc.* **2002**, *149*, G77- G84.

(45) The Bohr exciton radius is calculated by $r_B = (\epsilon_{dot}/\mu)a_B$, where $\mu = 1/(m^{*-1}_e + m^{*-1}_h)$, a_B is the hydrogen Bohr radius, ϵ_{dot} is the dielectric constant of the bulk material, and m^*_e and m^*_h are the reduced masses of the electron and hole. Values for $CuInS_2$ (m^*_e = 0.16, m^*_h = 1.3, and ϵ_{dot} = 11) and $CuInSe_2$ (m^*_e = 0.82, m^*_h = 0.71, and ϵ_{dot} = 14.7 ± 1.3) were obtained from refs 22 and 46, respectively.

(46) Rincón, C.; Márquez, R. *J. Phys. Chem. Solids.* **1999**, *60*, 1865−1873.